PHYSICAL REVIEW E **76**, 035402(R) (2007)

Acceleration dynamics of ions in shocks and solitary waves driven by intense laser pulses

Min-Qing He, Quan-Li Dong, Zheng-Ming Sheng,* Su-Ming Weng, Min Chen, Hui-Chun Wu, and Jie Zhang
Beijing National Laboratory of Condensed Matter Physics, Institute of Physics, CAS, Beijing 100080, China
(Received 17 April 2007; revised manuscript received 9 July 2007; published 19 September 2007)

The acceleration of ions in collisionless electrostatic shocks and solitary waves, driven by ultrashort intense laser pulses in a thin solid target under different conditions, is investigated theoretically. When a shock is formed, ions with certain initial velocities inside the target can be accelerated by the electrostatic field at the shock front to twice the shock speed. When a solitary wave is formed, only ions located at the rear surface of the target can be accelerated by the solitary wave together with the sheath field formed there.

DOI: 10.1103/PhysRevE.76.035402 PACS number(s): 52.38.Kd, 41.75.Jv, 52.65.Rr

The generation of high-flux energetic ion beams with short intense laser pulses has been a subject attracting wide attentions in recent years. Such beams may find applications in the fast ignition of fusion targets [1], radiography [2], medical applications [3], compact particle accelerators [4–6], etc. Energetic ions from laser-plasma interactions are usually accelerated by quasistatic electric fields due to space charge separation, which are induced at the front of the target when the laser ponderomotive force pushes electrons forward and backward at the interacting region [6,7]. The quasistatic electric fields also exist in the rear sheath due to different temperatures between electrons and ions [4].

It is shown that ions located deep in plasmas can also be accelerated by electrostatic shock waves. The formation of collisionless electrostatic shocks (CESs) and their capabilities of accelerating ions were studied both theoretically and experimentally in plasma stream collisions or intense laser-plasma interactions [8–15]. For example, Sliva *et al.* found from particle-in-cell (PIC) simulations that the shock wave acceleration of ions can even dominate the sheath acceleration in the target rear when the target thickness is under a certain threshold determined by the intensity of the incident laser pulses [11].

In this Rapid Communication, we report our studies on the formation of the CESs by PIC simulations under various conditions. The circulation of hot electrons between the front and the rear surfaces of the target was considered to explain the dependence of the shock speed on target thickness. Solitary waves can also be produced under different conditions. Even though ions can be accelerated by both kinds of waves, the involved acceleration processes are different.

We have used both one-dimensional (1D) and two-dimensional (2D) PIC simulations [16] to study the shocks and the solitary waves in overdense plasma foils with various thicknesses of L, placed in the middle of the simulation boxes with a vacuum space of 7 μm at the left side. Circularly or linearly s-polarized laser pulses are incident from the left boundary with a sine-squared temporal profile at different durations τ. The laser wavelength is $\lambda_0=1$ μm. We have adopted different plasma densities, target thicknesses, and incident laser intensities represented by the dimensionless variable $a_0^2=I\lambda_0^2/(1.37\times10^{18}$ W cm^{-2} μm$^2)$. The ions are set as protons with the mass $m_i=1836m_e$ in all simulations. For the 2D case, the simulation box is set as 16×15 μm^2. In the transverse y direction, laser beams have Gaussian intensity distributions with the diameter of 5 μm.

Figure 1(a) plots a typical ion distribution in the longitudinal phase space when a CES is formed. In this 2D simulation, $a_0=5$, $n_0=20n_c$, and $L=1.5\lambda_0$. The pulse duration is 200 laser periods τ_0. The shock front locates at $x=7.5\lambda_0$ at $t=30\tau_0$, which moves at a speed of about $u_s=0.03c$. Some ions are trapped and reflected at twice of the shock speed, which plays the role of the dissipation in the formation of the shock wave. The ion reflection is an indication of the shock formation. We have followed the trajectory of a test ion trapped and accelerated by the shock wave. This ion locates initially at $x=7.58\lambda_0$. When the shock front arrives, it is trapped and accelerated quickly to $0.06c$ as represented by open circles in Fig. 1(a). Then this ion moves forward with the same speed until it arrives at the rear of the target, where it is accelerated again in the sheath field. As a comparison, Fig. 1(b) plots the ion phase space obtained in another 2D simulation with the electron density decreased to $10n_c$ and other parameters the same as in Fig. 1(a). A solitary wave forms rather than a shock. The main difference between Figs. 1(a) and 1(b) is that, in Fig. 1(b), there is no ion trapping and reflection at the wave front. For example, a test ion located initially at $x=7.59\lambda_0$ is pushed to $0.04c$ at $t=30\tau_0$ as represented by open squares; but later it loses most of its momentum although it is displaced by 0.5 μm.

Simulations indicate that the plasma foil thickness and the initial target density have significant effects on the shock characteristics, since both of them affect the absorption of the incident laser pulse and the electron temperature. Figure 1(c) plots the mach number and the initial shock speed versus target thicknesses with different laser intensities and polarizations applied. The symbols of pluses and crosses represent the initial shock speeds from 1D PIC simulations with circularly polarized laser pulses of $a_0=16$ and 5, and $n_0=10n_c$ and $20n_c$, respectively. It is noted that the shock speed decreases rapidly when the target thickness increases until about $5\lambda_0$, and then it changes slowly with the further increase of the target thickness. This trend can be explained by the momentum-conservation model taking into account the motion of hot electrons circulating between the front and the rear surface of the target. According to Denavit's model [17], we have $m_i v_p^2 n_{i,eff}=I(1+\eta)/c$, where the original ion

*zmsheng@aphy.iphy.ac.cn

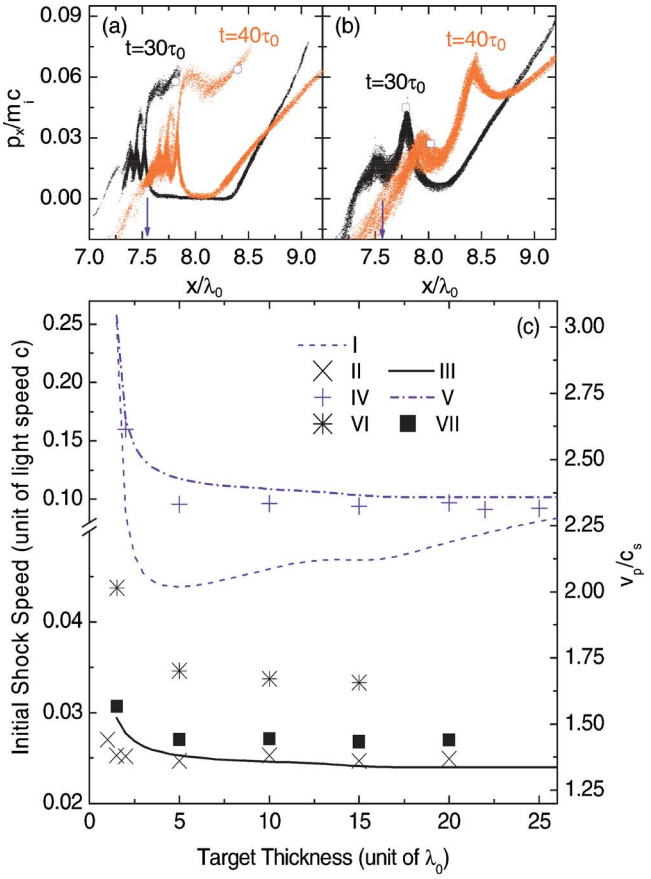

FIG. 1. (Color online) Snapshots showing the distribution of ions in the longitudinal phase space p_x at $t=30\tau_0$ and $40\tau_0$. (a) The case when a shock wave is formed for $a_0=5$, $n_0=20n_c$, and $L=1.5\lambda_0$. A test ion located initially near $x=7.58\lambda_0$ (marked by arrows) is accelerated by the shock wave as marked by the open circles for different time. (b) The case when a solitary wave is formed for $a_0=5$, $n_0=10n_c$, and $L=1.5\lambda_0$. A test ion marked by open squares is not accelerated efficiently by the solitary wave. Plot (c) shows the initial shock speed and the Mach number versus target thicknesses, where line I represents the calculated Mach number; lines II and III are the shock speeds from 1D PIC simulations and model calculation, respectively, for a circularly polarized laser pulse of $a_0=5$ and plasma density $n_0=20n_c$; lines IV and V are similar to lines II and III, respectively, but with $a_0=16$ and $n_0=10n_c$; and lines VI and VII are shock speeds found by 2D PIC simulations with circular and linear polarized laser pulses, respectively, at $a_0=5$ and $n_0=20n_c$.

density n_i is replaced by $n_{i,eff}=n_i\{1-l_p/L\exp[-(L/L_c)^q]\}$ because the energetic electrons can circulate back to the target front and not all ions are pushed forward and accelerated along with the intense laser pulse. The exponential factor $\exp[-(L/L_c)^q]$ is used to take into consideration the effects of the target thickness on the number of the electrons returning from the rear back to the front. Then the initial shock speed is defined as $v_p=\sqrt{(1+\eta)I/(m_i n_{i,eff}c)}$ and $L_c=c\tau/2$ is the critical target thickness for the accelerated electron to finish one cycle between the front and the rear. The laser sweeping length can be estimated by the local plasma Debye length, that is $l_p \doteq \lambda_D=2\pi v_{th}/\omega_p(x)\doteq(2\pi c/\omega_0)\sqrt{\gamma_{os}n_c/n_0}$ [18]. In the calculation, we simply take $q=10$, assuming that no electrons circulate back when $L>L_c$. The dash-dot line and the solid line in Fig. 1(c) show the above two series of results calculated with the absorption ratio between 15% and 20% based upon the 1D PIC simulations. A quantitative agreement is found between the modified model and the numerical simulations. It is also noted that the effects of multidimensions and laser polarizations may play important roles in determining the shock speeds. In Fig. 1(c), the stars and the closed squares represent results from 2D PIC simulations with circularly and linearly polarized laser pulses, respectively, at $a_0=5$ and $n_0=20n_c$. Both the two series of 2D results indicate a higher shock speed than the 1D case due to the side effect of electron compensation in the 2D geometry. Note that the shock speed in the circular polarization case is roughly $\sqrt{2}$ times that in the linear case, which agrees with the difference of the light momentum transfer in the two cases with the same a_0.

The Mach number of the shock waves is also studied with the heated plasma treated as a two-temperature fluid. Then the effective temperature is $T_{eff}=T_hT_l/(\mu T_h+\nu T_l)$, where $\nu=l_p/L$, $\mu=L-l_p/L$, T_h is the hot electron temperature and equal to the ponderomotive potential $\phi_p=m_ec^2(\sqrt{a^2+1}-1)$, and T_l is the cold temperature roughly set as one-tenth of T_h. The acoustic wave of such a plasma can then be written as $c_s=\sqrt{ZK_BT_{eff}/m_i}$. The Mach number $M=v_p/c_s$ versus the target thickness is given in Fig. 1(c) as the dashed line, which shows a rapid decrease and then a slow increase with increasing target thickness. It is worthy to point out that although the presented results from the PIC simulations and the analytical model show qualitative agreement with the 1D PIC simulations by Silva *et al.*, our result does not show apparent dependence on the critical target length L_c as implied by Fig. 2 in Ref. [11]. In that work, for the used laser pulse of $\tau_{laser}=100$ fs, the shock speed and the Mach number change their trend versus the target thickness at $L=L_c=15$ μm.

Figures 2 and 3 show the detailed acceleration process of ions in shocks and solitary waves. Figure 2(a) shows the ion density distribution at $t=40\tau_0$ in the coordinate space with simulation parameters the same as in Fig. 1(a). At the first stage, the laser pulse compresses the thin layer target at the front surface and drives it forward with a speed of v_p. The space-time evolution of the plasma density and the incident laser field at position $y=7.5\lambda_0$ is shown in Fig. 2(b), where the contour is the plot of the ion density at $n_i=45n_c$. One can see that the shock front slowly separates from the laser field, which propagates forward even without the further push of the laser ponderomotive force. This differs from the ion acceleration in the radiation-pressure dominated regime [10]. The peaks of the ion and electron densities overlap with each other as shown in Fig. 2(c). This distinguishes the shock acceleration process from the ion acceleration at the target front, where the charge separation field is formed due to the laser push of the front electron layer [6,19]. In the situations of shock acceleration, bipolar charge separation fields are produced in the Debye sheath of the compressed plasma layer because of different electron and ion temperatures of the compressed plasma layer. A bunch of ions accelerated can be seen clearly in Fig. 2(d).

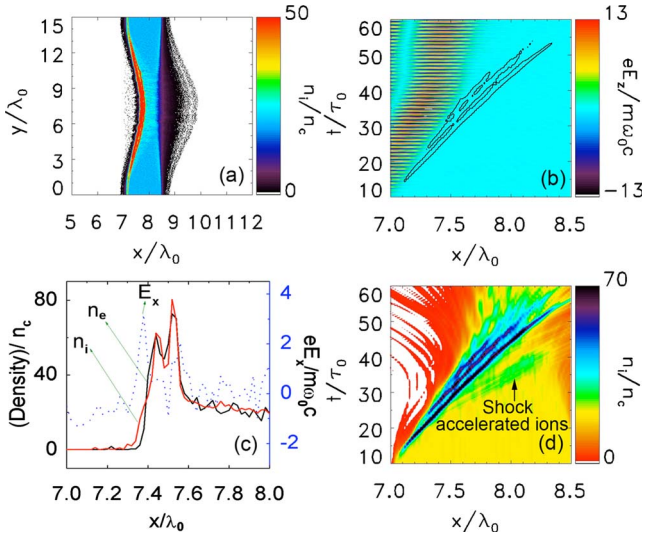

FIG. 2. (Color online) (a) Snapshot of the ion density in 2D space at $t=40\tau_0$. (b) The space-time evolution of the laser fields (E_z). The ion density contour lines of $45n_c$ are also overplotted. (c) The longitudinal density distributions of the ions and electrons, and the longitudinal electric field on the laser axis at $t=30\tau_0$. (d) The space-time evolution of the ion density distribution on the laser axis. The used parameters are the same as in Fig. 1(a).

Ion dynamics in the shock is then determined by the bipolar electric field. Figure 3(a) plots the longitudinal electric field E_x experienced by a test ion and its longitudinal momentum p_x versus time. The initial position of the test ion is $x=7.58\lambda_0$, which is inside the plasma and the laser field cannot penetrate there. The ion experiences a large electrostatic

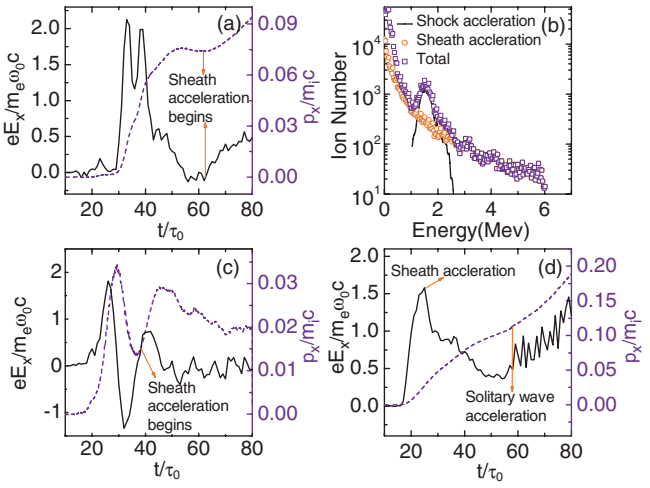

FIG. 3. (Color online) (a) The longitudinal field (E_x) experienced by an accelerated ion and its longitudinal momentum (p_x) (dashed line) as functions of time. (b) The ion energetic spectra accelerated by the shock wave and the sheath field, and their summed spectrum. The simulation parameters for (a) and (b) are the same as in Fig. 1(a). (c) The E_x experienced by an ion located initially inside plasma and its p_x (dashed line) as functions of time. (d) The E_x experienced by an ion located initially at the rear side and its p_x (dashed line) as functions of time. The simulation parameters for (c) and (d) are the same as in Fig. 1(b).

field between $t=29\tau_0$ and $43\tau_0$, during which the ion is reflected and divorced from the shock front, and obtains a speed of $2u_s=0.0623c$. After $62\tau_0$ when the shock-accelerated ion arrives at the target rear, the ion speed ascends again due to the sheath acceleration, as also indicated by the experienced electric field shown in the same plot. The energy distribution of the accelerated ions is given by Fig. 3(b). The ions accelerated by the sheath field show a wide energy spread [20], while the ion spectra accelerated by shocks, superimposed upon the previous one, have a relatively small energy spread. The latter is broadened after the shock propagates over a longer distance in the target due to the shock energy dissipation and shock speed decreasing.

However, simulation results indicate that not all the ions located in the path of the shocks can be accelerated. One may have noted that there is a dip on the top of the experienced electric field in Fig. 3(a). This is because the monitored ion passed twice the peak of the positive electric part. If the ion speed in the forward direction is still smaller than the shock speed after the acceleration in the positive shock field, it will fall into the negative part of the shock electric field, and loses its energy obtained before. This ion is not trapped and accelerated by the shock finally. For ions to be reflected, their initial speed u in the shock wave frame should satisfy $\frac{1}{2}m_i u^2 < \phi$, where $\phi=eE\lambda_D$ is the potential corresponding to the positive part of the shock electric field, $E=k_B T_e/e\lambda_D$ is the electric field strength within Debye length λ_D, and k_B is the Boltzmann constant. The above equation leads to $u>-\sqrt{2k_B T_e/m_i}$, which is $u>-0.001c$ for simulation parameters applied. This is verified in our simulation when checking hundreds of ions accelerated by shocks.

As a comparison, we examine the ion acceleration by the solitary wave. We found that only ions located at the target rear can be accelerated by the solitary wave combined with the sheath-field. Figure 3(c) shows the evolution of p_x of a test ion initially located in the middle of the plasma foil and the experienced E_x as shown by open squares in Fig. 1(b). This ion experiences a sine-like field, thus its velocity ascends first and then descends afterwards. If there is no other acceleration mechanisms, the ion will finally keep its energy similar to the original one although it may be displaced from its original position. When following a large number of ions located in the middle of plasma foils, we find that all of them have similar behavior in the solitary wave and they obtain no net energy. To obtain net energy, ions accelerated by the positive part of the electric field have to be extracted out of the solitary wave immediately after its acceleration process. This occurs for ions initially located at the target rear, where the solitary wave dissipates abruptly. The evolution of p_x and the experienced E_x for such a kind of ions is presented in Fig. 3(d). The ion is initially located 0.058 μm from the target rear surface. It is accelerated first by the sheath field while the plasma expands. The solitary wave formed at the front surface propagates at a high velocity through the plasma, catches the preaccelerated ions and accelerates them to a higher energy.

The temporal and spatial evolution of the electric field structure of the shock and the solitary waves cut at $y=7.5\lambda_0$ are plotted in Fig. 4. In the case with shock formation shown in Fig. 4(a), the shock is found to propagate

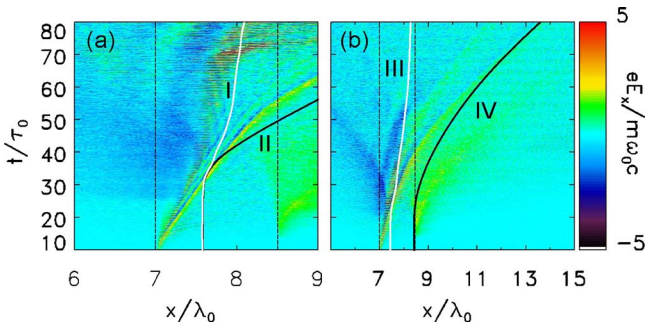

FIG. 4. (Color online) (a) The space-time evolution of the longitudinal electrostatic field (E_x) along the laser axis. Two ion trajectories are also overplotted with one (marked II) accelerated by the shock wave and another (marked I) not accelerated. The simulation parameters are the same as in Fig. 1(a). (b) The space-time evolution of E_x along the laser axis. Two ion trajectories are shown with one (marked IV) accelerated by the solitary wave together with the sheath field, and another (marked III) not accelerated. The simulation parameters are the same as in Fig. 1(b). The dashed lines are the initial boundaries of the plasma targets.

almost with a constant speed until it reaches the rear surface of the target. In the case with the solitary wave formation shown in Fig. 4(b), the wave speed tends to increase slightly with time. The trajectories of some test ions are also plotted in Fig. 4 to show the combined acceleration by the shock or solitary waves and the sheath field. Curve II in Fig. 4(a) represents the trajectory of an ion accelerated by the shock wave. Curve IV in Fig. 4(b) is an example of ions first accelerated in the sheath field, and then further accelerated by the solitary wave arriving at the rear surface of the target.

In summary, a parametric study was performed with PIC simulations about the formation of the shock wave and solitary wave driven by short intense laser pulses. A model based on the momentum conservation was invoked to explain the dependence of shock speed on the target thickness by including the effects of the hot electron circulation between the front and rear sides. When a shock wave is formed, the accelerated ion energy spectrum shows a quasimonoenergetic peak, which is superimposed upon that produced by the sheath field. We also found that the solitary wave can accelerate ions only located at the rear surface of the target. The ion bunches produced by the shock wave have both narrow energy spread and ultrashort pulse durations, which may be suitable for some applications such as proton beam radiography and an injector of ion accelerators.

This work was supported by the Natural Science Foundation of China (Grant Nos. 10425416, 10335020, 10575129, 10674175, and 10774184), the CAS project KJCX2-YW-T01, and the National High-Tech ICF Committee of China.

[1] M. Roth *et al.*, Phys. Rev. Lett. **86**, 436 (2001).
[2] M. Borghesi *et al.*, Phys. Plasmas **9**, 2214 (2002); Y. Glinec *et al.*, Phys. Rev. Lett. **94**, 025003 (2005).
[3] E. Lefebvre *et al.*, J. Appl. Phys. **100**, 113308 (2006).
[4] L. Romagnani *et al.*, Phys. Rev. Lett. **95**, 195001 (2005); A. J. Mackinnon *et al.*, *ibid.* **88**, 215006 (2002); J. Badziak *et al.*, *ibid.* **87**, 215001 (2001); A. Maksimchuk, S. Gu, K. Flippo, D. Umstadter, and V. Y. Bychenkov, *ibid.* **84**, 4108 (2000); R. A. Snavely *et al.*, *ibid.* **85**, 2945 (2000).
[5] S. P. D. Mangles *et al.*, Phys. Rev. Lett. **96**, 215001 (2006), and references therein.
[6] M. Kaluza *et al.*, Phys. Rev. Lett. **93**, 045003 (2004); E. L. Clark *et al.*, *ibid.* **84**, 670 (2000).
[7] J. Schreiber *et al.*, Phys. Rev. Lett. **97**, 045005 (2006); P. Mora, *ibid.* **90**, 185002 (2003), and references therein.
[8] D. W. Forslund and C. R. Shonk, Phys. Rev. Lett. **25**, 1699 (1970); D. W. Forslund and J. P. Freidberg, *ibid.* **27**, 1189 (1971).
[9] G. Sorasio, M. Marti, R. Fonseca, and L. O. Silva, Phys. Rev. Lett. **96**, 045005 (2006).
[10] W. Yu *et al.*, Phys. Rev. E **72**, 046401 (2005); T. Esirkepov, M. Borghesi, S. V. Bulanov, G. Mourou, and T. Tajima, Phys. Rev. Lett. **92**, 175003 (2004).
[11] L. O. Silva *et al.*, Phys. Rev. Lett. **92**, 015002 (2004).
[12] H. Habara *et al.*, Phys. Rev. E **70**, 046414 (2004).
[13] M. S. Wei *et al.*, Phys. Rev. Lett. **93**, 155003 (2004).
[14] A. Zhidkov, M. Uesaka, A. Sasaki, and H. Daido, Phys. Rev. Lett. **89**, 215002 (2002).
[15] N. Izumi *et al.*, Phys. Rev. E **65**, 036413 (2002).
[16] Z.-M. Sheng *et al.*, Phys. Rev. Lett. **85**, 5340 (2000); Z.-M. Sheng, H. C. Wu, K. Li, and J. Zhang, Phys. Rev. E **69**, 025401(R) (2004).
[17] J. Denavit, Phys. Rev. Lett. **69**, 3052 (1992); S. C. Wilks, W. L. Kruer, M. Tabak, and A. B. Langdon, *ibid.* **69**, 1383 (1992).
[18] Q. L. Dong, Z. M. Sheng, M. Y. Yu, and J. Zhang, Phys. Rev. E **68**, 026408 (2003); Y. Sentoku *et al.*, Phys. Plasmas **10**, 2009 (2003).
[19] A. Macchi, F. Cattani, T. V. Liseykina, and F. Cornolti, Phys. Rev. Lett. **94**, 165003 (2005).
[20] V. Y. Bychenkov *et al.*, JETP **88**, 1137 (1999).